ACS NANO

www.acsnano.org

ARTICLE

Large-Area Nanogap-Controlled 3D Nanoarchitectures Fabricated *via* Layer-by-Layer Nanoimprint

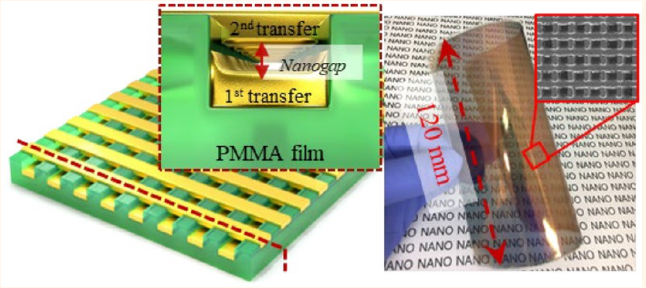
Zhi-Jun Zhao, Junseong Ahn, Soon Hyoung Hwang, Jiwoo Ko, Yongrok Jeong, Moonjeong Bok, Hyeok-Joong Kang, Jungrak Choi, Sohee Jeon, Inkyu Park,* and Jun-Ho Jeong*

Cite This: *ACS Nano* 2021, 15, 503−514

Read Online

ACCESS | Metrics & More | Article Recommendations | Supporting Information

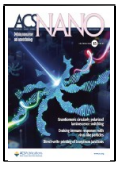
ABSTRACT: The fabrication of large-area and flexible nanostructures currently presents various challenges related to the special requirements for 3D multilayer nanostructures, ultrasmall nanogaps, and size-controlled nanomeshes. To overcome these rigorous challenges, a simple method for fabricating wafer-scale, ultrasmall nanogaps on a flexible substrate using a temperature above the glass transition temperature (T_g) of the substrate and by layer-by-layer nanoimprinting is proposed here. The size of the nanogaps can be easily controlled by adjusting the pressure, heating time, and heating temperature. In addition, 3D multilayer nanostructures and nanocomposites with 2, 3, 5, 7, and 20 layers were fabricated using this method. The fabricated nanogaps with sizes ranging from approximately 1 to 40 nm were observed via high-resolution transmission electron microscopy (HRTEM). The multilayered nanostructures were evaluated using focused ion beam (FIB) technology. Compared with conventional methods, our method could not only easily control the size of the nanogaps on the flexible large-area substrate but could also achieve fast, simple, and cost-effective fabrication of 3D multilayer nanostructures and nanocomposites without any post-treatment. Moreover, a transparent electrode and nanoheater were fabricated and evaluated. Finally, surface-enhanced Raman scattering substrates with different nanogaps were evaluated using rhodamine 6G. In conclusion, it is believed that the proposed method can solve the problems related to the high requirements of nanofabrication and can be applied in the detection of small molecules and for manufacturing flexible electronics and soft actuators.



KEYWORDS: *3D multilayer nanostructures, nanogaps, layer-by-layer nanoprint, surface-enhanced Raman scattering, glass transition temperature*

Next-generation nanofabrication is important to achieve the exigent requirements of various applications such as optical devices,[1,2] chemical sensors,[3,4] metamaterials,[5] and surface-enhanced Raman scattering (SERS) technology.[6−8] Conventional methods including lithography,[9,10] laser direct writing,[11] and nanotransfer printing[12,13] have been widely applied to fabricate various nanostructures. Among them, lithography allows high resolution and large-area nanofabrication; however, it is expensive and time-consuming, because of which it has limited application (it is only suitable for high-value products including memory chip and integrated circuits). In contrast, nanoimprint lithography (NIL) can solve the issues of lithography, such as high cost, time consumption, and large-area nanofabrication, *via* the roll-to-roll method. The residual layer, however, is a bottleneck for large-area fabrication without any defects for specialized applications. In addition, it is difficult to achieve a high resolution such as that obtained by e-beam lithography (EBL) *via* NIL. Therefore, some methods have been developed to address these problems; recently, Hwang *et al.* proposed a covalent bonding-assisted nanotransfer method to fabricate high-resolution nanostructures at a low cost.[14] In addition, Jeong *et al.* transferred Au, Ag, and Pd nanowires onto diverse surfaces based on a solvent-dissolvable polymer master mold and using a solvent-assisted nanotransfer printing method.[15] Seo *et al.* reported a material-

Received: June 26, 2020
Accepted: January 12, 2021
Published: January 13, 2021



Downloaded via KOREA ADVANCED INST SCI AND TECHLGY on November 21, 2022 at 13:48:17 (UTC).
See https://pubs.acs.org/sharingguidelines for options on how to legitimately share published articles.

© 2021 American Chemical Society

https://dx.doi.org/10.1021/acsnano.0c05290
ACS Nano 2021, 15, 503−514

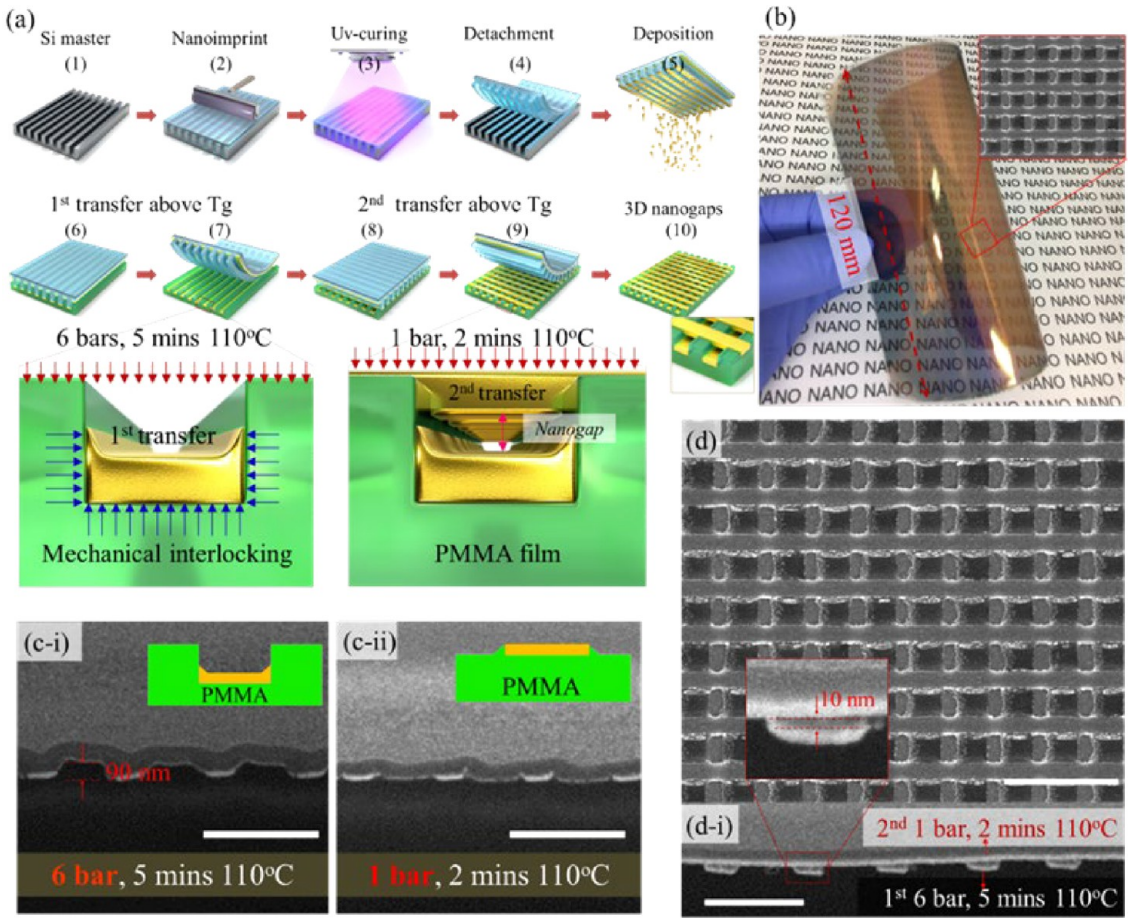


Figure 1. Fabrication process, morphologies, and cross-sectional images of the nanogaps produced on the wafer-scale, flexible substrate. (a) Fabrication process: (1)−(4) replication of the polymer mold *via* nanoimprinting and ultraviolet (UV)-curing; (5) metal deposition; (6) and (7) first metal transfer at a temperature above the *Tg* of the substrate (specific conditions shown in the magnified image); (8) and (9) second transfer at a temperature above the *Tg* of the substrate (specific conditions shown in the magnified image); (10) formation of the 3D nanogaps. (b) Photograph of the nanogaps (scanning electron microscopy images shown in the inset). (c-i) and (c-ii): Cross-sectional images of the samples after transfer under different conditions. (d) and (d-i): Morphology and cross-sectional image of the nanogaps.

independent mechanical interlocking method to fabricate ultralong and fully aligned nanowires on a large flexible substrate.[16] These methods can overcome the limitations related to large-area nanofabrication, which is an expensive and time-consuming process, on flexible substrates. However, special nanostructures need to be fabricated using desirable methods for attaining high performance for specific applications. Among the nanostructures fabricated *via* various methods, metal nanostructures with an ultrasmall nanogap have been widely applied for the detection of molecules present in extremely low amounts. Surface-enhanced Raman scattering analysis has been considered as one of the most practical technologies for this purpose.[17−21] This technique can enhance Raman scattering by molecules adsorbed on rough metal surfaces or by plasmonic nanostructures such as typical gold and silver nanostructures.[22−24] In previous studies, plasmonic cavity arrays,[25,26] plasmonic nanoparticle arrays,[27,28] plasmonic nanogap arrays,[29,30] and plasmonic silver supercrystals[31] for SERS substrates have been fabricated by nanosphere lithography (NSL), an angle evaporation technique, EBL, and a nanocasting method, respectively. In these studies, ultrasmall nanogaps for high-performance, SERS-based molecule detection were created. However, complex post-treatments were required during the fabrication process such as anisotropic etching, focused ion beam (FIB) milling, and chemical cleaning. To improve these points, wafer-scale, ultrasmall nanogaps fabricated on a flexible poly(methyl methacrylate) (PMMA) film were developed based on heating above the glass transition temperature (*Tg*) of the polymer and using the layer-by-layer nanoimprint method. Noble metal nanowires were deposited on the polymer mold using an e-beam evaporator. The fabricated metal nanowires were successively transferred onto the PMMA substrate by heating above the *Tg* of the polymer, thereby forming up−down nanogaps of the cross structures. The nanogaps could be controlled by adjusting the applied pressure, heating time, and heating temperature. The fabricated nanostructures were observed by FIB and transmission electron microscopy (TEM). In addition, multilayers without any defects could be fabricated based on the *Tg* of the substrate and nanowelding technology. Interestingly, the PMMA substrate played an important "cushioning" role during the process of the layer-by-layer method. Here, a PMMA film with the thickness of 150 μm was chosen as the substrate to achieve nanotransfer. Three, five, seven, and 20 layers were fabricated using the proposed method. We found that the PMMA substrate became thinner with increasing transfer metal layers due to the repeated process of pressure application and

https://dx.doi.org/10.1021/acsnano.0c05290
ACS Nano 2021, 15, 503−514

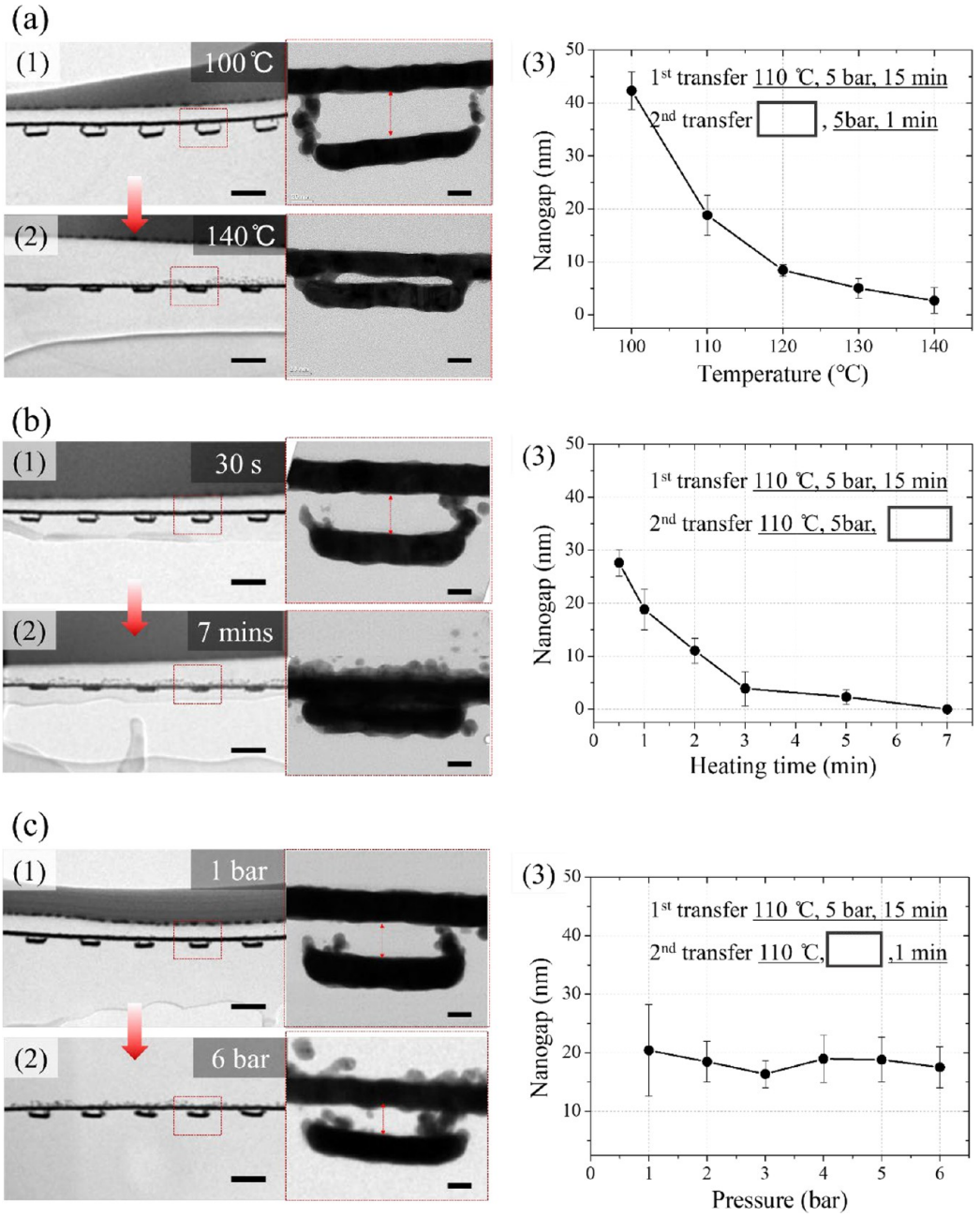


Figure 2. TEM cross-sectional images and diversification of the fabricated nanogaps depending on the heating temperature, heating time, and pressure. (a) Nanogaps fabricated at different heating temperatures: (1) first transfer at 5 bar and 110 °C for 15 min and second transfer at 5 bar and 100 °C for 1 min; (2) first transfer at 5 bar and 110 °C for 15 min and second transfer at 5 bar and 140 °C for 1 min; (3) various nanogaps of the second transfer depending on the heating temperature from 100 to 140 °C. (b) Nanogaps fabricated under different heating times: (1) First transfer at 5 bar and 110 °C for 15 min and second transfer at 5 bar and 110 °C for 30 s; (2) first transfer at 5 bar and 110 °C for 15 min and second transfer at 5 bar and 110 °C for 7 min; (3) the variety of nanogaps depending on the heating temperature of the second transfer from 30 s to 7 min. (c) Nanogaps fabricated at different pressures: (1) first transfer at 5 bar and 110 °C for 15 min and second transfer at 1 bar and 110 °C for 1 min; (2) first transfer at 5 bar and 110 °C for 15 min and second transfer at 6 bar and 110 °C for 1 min; (3) the variety of nanogaps depending on the pressure of the second transfer from 1 to 6 bar.

heating. Compared with conventional methods, our method could not only achieve the modulation of nanogaps on a large-area, flexible substrate in a simple manner but also allowed for the successful fabrication of multilayer nanostructures. Moreover, mesh nanostructures with different sizes were fabricated using the layer-by-layer method. A transparent electrode and a heater with the size of 1600 nm × 1600 nm were evaluated. Lastly, the SERS properties of the nanogaps in the different fabricated nanostructures were evaluated. Our method can be of significance in various applications such as fabrication of plasmonic, flexible, and wearable devices and in SERS sensing.

RESULTS AND DISCUSSION

To fabricate the nanogaps on the wafer-scale substrate, the layer-by-layer nanoimprint method was used to achieve the transfer of the metal nanostructures onto the receiver substrate (PMMA) by heating above the *Tg* of the polymer. In this work, Au nanowires were fabricated using nanoimprint and e-

https://dx.doi.org/10.1021/acsnano.0c05290
ACS Nano 2021, 15, 503−514

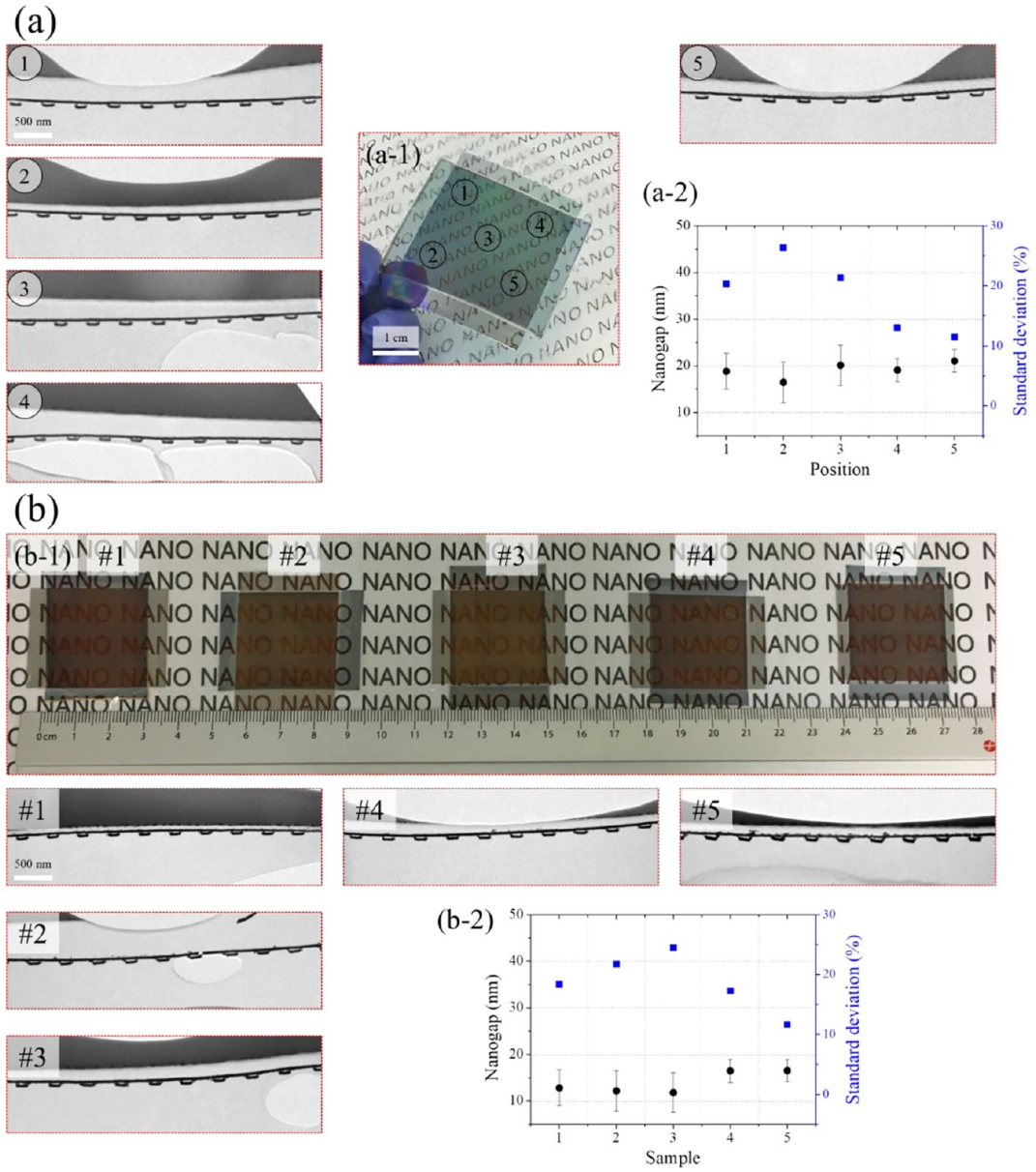


Figure 3. Evaluation of the uniformity and reproducibility of the nanogaps fabricated using the proposed method. (a) Uniformity of nanogaps observed *via* TEM cross-sectional images at (a-1) five different positions of the substrate fabricated under the condition of first transfer at 5 bar and 110 °C for 15 min and second transfer at 5 bar and 110 °C for 1 min. (a-2) The variety of nanogaps based on different positions. (b) Reproducibility observed *via* TEM cross-sectional images of (b-1) five samples fabricated under the same conditions of first transfer at 5 bar and 110 °C for 5 min and second transfer at 5 bar and 110 °C for 1 min. (b-2) The variety of nanogaps based on the different samples.

beam evaporation (see Figure 1a [steps 1−5]), which were transferred onto the PMMA film by heating above the *Tg* of the substrate (see Figure 1a [steps 6 and 7]). The nanofabrication process is detailed in the Experimental Section. Compared with the conventional transfer method, our method does not require any chemical adhesive coating layer; it can be performed by simply heating above the *Tg* of the polymer. As it is known, the *Tg* is the temperature below which the physical properties of plastics change from those of a glassy state to those of a crystalline state. Above the *Tg*, they behave like rubbery materials and are more mobile. In previous studies, PMMA resin and films were widely applied to fabricate polymer micro/nanopatterns using the thermal nanoimprint method.[32−34] In addition, many researchers have reported the deformation of PMMA resin and films when heated above their *Tg*, depending on the applied pressure and heating time.[35,36] According to the aforementioned studies, size-controlled nanogaps were fabricated by heating above the *Tg* of PMMA and by adjusting the applied pressure and heating time. The nanofabrication process is illustrated in Figure 1a. The nanogaps fabricated on the large-area, flexible substrate are displayed in Figure 1b (the morphology is shown in the inset). A 120 mm × 120 mm specimen is presented Figure 1b. The large-area sample with a standard ruler is shown in Figure S1, which clearly displays the size of the large nanofabricated area. Figure 1c shows a schematic representation of the nanogaps at different values of pressure and heating time. First, the transfer was performed at 110 °C, 6 bar, and a heating time

https://dx.doi.org/10.1021/acsnano.0c05290
ACS Nano 2021, 15, 503−514

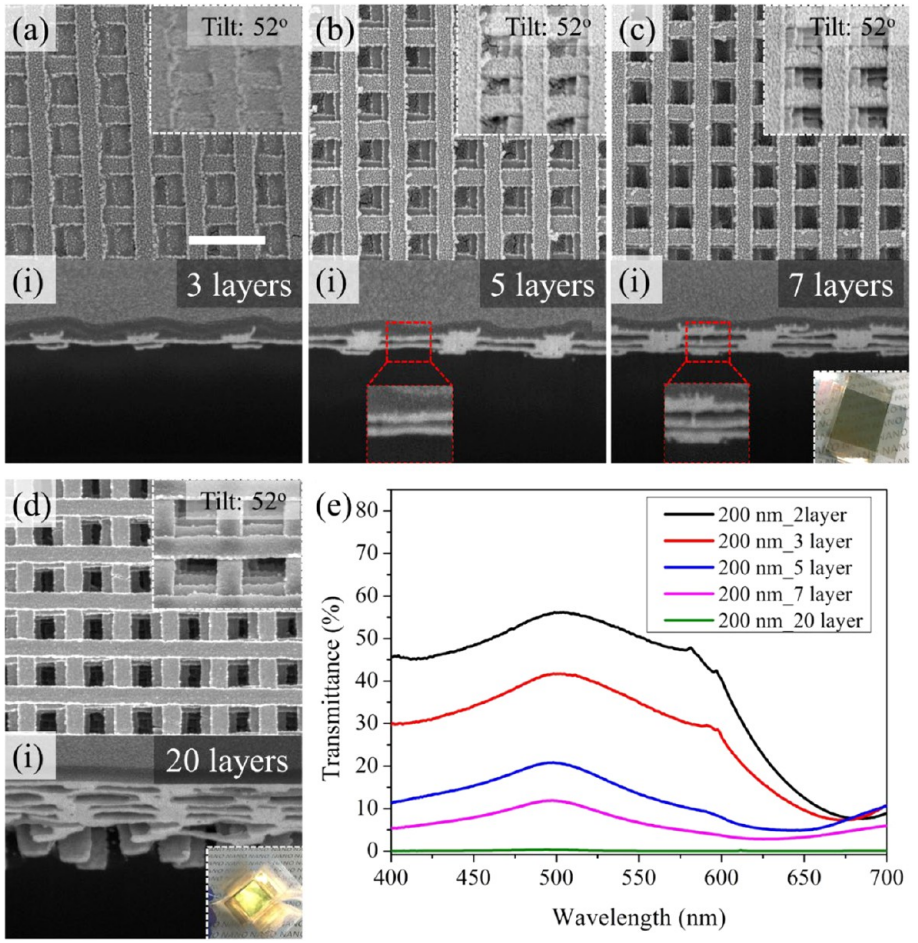


Figure 4. Morphologies and cross-sectional images of the multilayer nanostructures and their corresponding transmittance variations. (a) and (a-i) Morphology and cross-sectional images of the three-layered nanostructure. (b) and (b-i) Morphology and cross-sectional images of the five-layered nanostructure. (c) and (c-i) Morphology and cross-sectional images of the seven-layered nanostructure. (d) and (d-i) Morphology and cross-sectional images of the 20-layered nanostructure. (e) Corresponding transmittance variations.

of 5 min to produce deeply imprinted Au nanowires, thus forming the nanochannels. This could be achieved because the mechanical interlocking force (blue arrows in Figure 1a) separated the Au nanowires from the donor substrate, and the applied pressure and heating time promoted the formation of nanochannels after cooling. The cross-sectional image corresponding to these conditions is displayed in Figure 1c-i. In the second transfer, the nanogaps were formed at 110 °C, 1 bar, and a heating time of 2 min. According to the deformation of PMMA above its *Tg* and based on the pressure and heating time, a pressure of 1 bar and a heating time of 2 min were chosen to fabricate the Au nanowires transferred onto the surface of the PMMA substrate, thereby forming the nanogaps. The cross-sectional image corresponding to these conditions is presented in Figure 1c-ii. By observing Figures 1c-i and 1c-ii, it is believed that the nanogaps can be controlled by adjusting the heating temperature, pressure, and heating time, based on previous research on PMMA deformation. Figure 1d shows the morphology and cross-sectional image of the fabricated sample. The nanogaps of about 10 nm can be observed in Figure 1d-i.

To better observe the sizes of the nanogaps, high-resolution transmission electron microscopy (HRTEM) was performed. Figure 2 presents the HRTEM images of the fabricated samples depending on the heating time, heating temperature, and pressure. To demonstrate the controllability of the fabricated nanogaps, we performed experiments by fixing the transfer conditions of the first layer and changing the variables of temperature, pressure, and time of the second layer, respectively. In this study, all first layers were transferred on the PMMA film under a heating temperature of 110 °C, a pressure of 5 bar, and heating time of 15 min. As the heating temperature of the second layer changed from 100 to 140 °C, the average sizes of the nanogaps were changed from 42.3 to 2.7 nm, as shown in Figure 2a. The sizes of the fabricated nanogaps were obtained by calculating the average value of middle points. Figure 2a-(1) and -(2) show the TEM cross-sectional images of nanogaps fabricated under 100 and 140 °C, respectively. The sizes of the nanogaps gradually reduced with increasing heating temperature, as shown in Figure 2a-(3). Similarly, as the heating time of the second layer increased from 30 s to 7 min, the average sizes of nanogaps changed from 27.6 to 0 nm, as shown in Figure 2b. Figure 2b-(1) and -(2) demonstrate the TEM cross-sectional images of the nanogaps fabricated under heating times of 30 s and 7 min, respectively. Figure 2b-(3) demonstrates that the sizes of nanogaps reduced with increasing heating time. Moreover, Figure 2c shows the changes in the nanogaps fabricated under different pressures. The representative cross-sectional images of the nanogaps were fabricated under pressures of 1 and 6 bar, respectively. Figure

https://dx.doi.org/10.1021/acsnano.0c05290
ACS Nano 2021, 15, 503−514

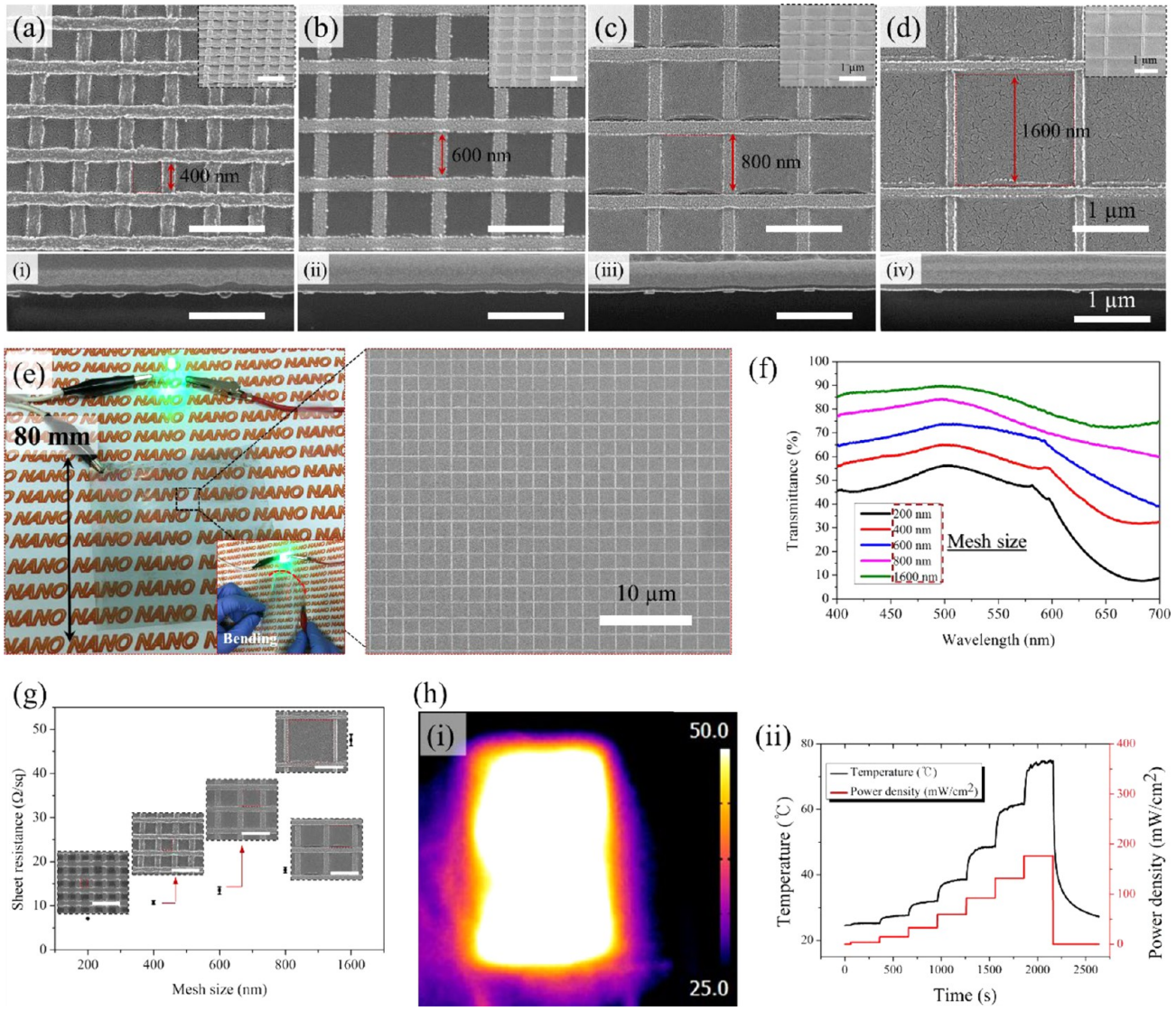


Figure 5. Nanomeshes of different sizes fabricated *via* the nanoimprinting method. (a–d) Morphologies of the 400 × 400 nm, 600 × 600 nm, 800 × 800 nm, and 1600 × 1600 nm nanomeshes. (a-i)–(d-iv) Corresponding FIB cross-sectional images. (e) Photograph of the transparent electrode with a 1600 × 1600 nm nanomesh (a photograph of the bent electrode is shown as an inset). (f) and (g) Transmittance and sheet resistance of the nanomeshes of different sizes. (h-i) Infrared image of the transparent nanoheater at 50 °C. (h-ii) Temperature variation with power density under constant time.

2c-(3) shows that the pressure did not significantly affect the nanogap size, and a gap change of less than 10% was observed when the pressure changed from 1 to 6 bar. Instead, the pressure affected the conformal contact, which is directly related with the gap uniformity between the PMMA substrate and the metal layer. Notably, the average standard deviation (STD) of the nanogaps was approximately 40% under 1 bar of pressure, which is not enough for conformal contact. However, it was reduced to 14% under 3 bar of pressure. Therefore, we can conclude that the pressure, heating time, and heating temperature have significant effects on the controllability of the nanogaps; this phenomenon is consistent with the results of previous studies[33,37] (when heated above their *Tg*, PMMA resin and films deform depending on the applied pressure, heating temperature, and heating time). In addition, the detail experimental conditions of the fabricated nanogaps are provided in Table S1. In addition, the specific change of the nanogaps depending on the heating temperature, heating time, and pressure (detail conditions) can be observed from the TEM cross-sectional images shown in Figure S2.

Furthermore, during the fabrication process, we found that proper cooling time is required for the formation of the parallel shape of nanogaps before implementing the detachment process (Figure 1a-(7) and -(9)). To evaluate the shape of nanogaps depending on the cooling time, cooling times of 1 and 5 min were implemented. The parallel nanogaps were fabricated due to recovery to the glassy state of PMMA after a sufficient cooling time of 5 min, as shown in Figure 2. When the cooling time was insufficient (approximately 1 min), triangular nanogaps were obtained due to the remaining rubbery PMMA substrate, as shown in Figure S3.

To ensure uniformity and reproducibility of the fabricated nanogaps, five different positions on the sample and five samples repeatedly fabricated using the same conditions were observed, and their TEM images were evaluated, as shown in Figure 3a and 3b, respectively. Figure 3a demonstrates the TEM cross-sectional images of five different positions on the

https://dx.doi.org/10.1021/acsnano.0c05290
ACS Nano 2021, 15, 503–514

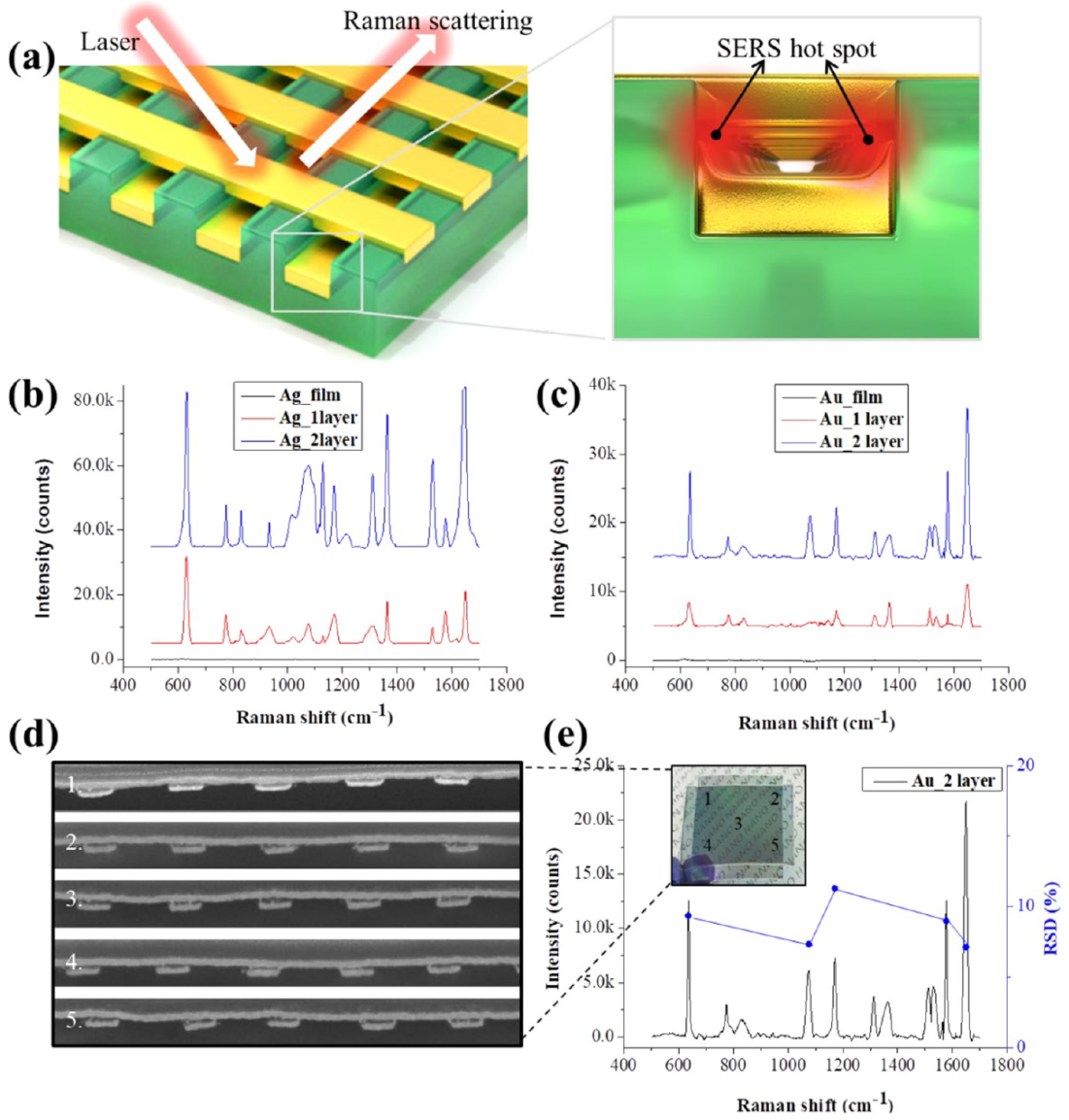


Figure 6. Performance and characterization of the developed nanogap array as an SERS substrate. (a) Schematic illustrations of the fabricated nanogap structure and hot spots. (b) SERS signals of the one-layer and two-layer Au lines. (c) SERS signals of the one-layer and two-layer Ag lines. (d) FIB-SEM images of the two-layer Au nanogap structures at five different points. (e) Raman intensity and RSD values of each of the five points at representative rhodamine 6G peaks.

sample (first transfer at 110 °C, 5 bar, and 15 min; second transfer at 110 °C, 5 bar, and 1 min). It can be seen that the average nanogap spacing of the five different regions (see Figure 3a-(1)) is highly uniform with a STD within 20.1% (see Figure 3a-(2)). Moreover, when the nanogap structure was fabricated five times repeatedly under the same process conditions (the first transfer at 110 °C, 5 bar, and 5 min and second transfer at 110 °C, 5 bar, and 1 min), as shown in Figure 3b-(1), the results exhibited a reasonable STD of 15.1%, as shown in Figure 3b-(2). Thus, we could conclude that the developed structure had sufficient potential for commercialization as a well-controlled reproducible nanogap substrate over large areas of multiple samples.

To create 3D multilayer nanoarchitectures, we fabricated the nanoarchitectures *via* the layer-by-layer nanoimprint method. Three-dimensional nanostructures have been widely applied in various fields such as biosensing,[38,39] catalysts,[40,41] and optics[42] because the enhanced surface area of these structures can be effectively used, compared with conventional nanostructures. Three-dimensional nanostructures have been mostly fabricated using conventional methods such as lithography, transfer printing, reactive-ion etching (RIE), and inductively coupled plasma (ICP) etching. However, these methods are time-consuming, present high costs, and are not suitable for large-area fabrication. In addition, Rogers *et al.*[43−45] reported the fabrication of multimetal nanostructures *via* a nanotransfer imprinting method which mainly utilized the weaker adhesion of PDMS due to its low surface energy and improved the adhesion of substrates *via* chemical surface treatment. However, in this study, a simple method for the fabrication of 3D metal nanostructures by heating above the *Tg* of the polymer film is proposed. Figure 4 presents the morphologies and cross-sectional images of the fabricated multilayer nanostructures (52° tilt images are shown as insets). The structures with 3, 5, 7, and 20 layers are presented in Figures 4a, 4b, 4c, and 4d, respectively. The corresponding cross-

https://dx.doi.org/10.1021/acsnano.0c05290
ACS Nano 2021, 15, 503−514

sectional images are displayed in Figures 4a-i, 4b-i, 4c-i, and 4d-i, respectively. The multilayers could be easily fabricated by layer-by-layer nanoimprinting; importantly, the first and second layers were sequentially transferred onto the PMMA film by heating above the *Tg* of PMMA at a constant pressure and heating time based on the mechanical interlocking force. In contrast, for the third layer, the Au nanowires were welded onto the top layer at 110 °C and 5 bar for 5 min, thereby forming a metallic bonding force; the welded layers can be observed in the cross-sectional images. To better understand the metallic bonding force of the metals, schematic and HRTEM cross-sectional images of the nanostructures with three layers are shown in Figure S4. The junction of the second and third Au layer can be observed in the HRTEM images (see Figure S4b-(3 and 4)). In previous studies, 3D metal nanostructures were developed *via* nanowelding technology.[46,47] However, the polymer mold had to be fabricated on PET or PMMA substrates using nanoimprinting resin. Therefore, defects could appear in the 3D metal nanostructures while fabricating the multilayer nanostructures due to repeated heating, and the bottom metal layer could be damaged. In contrast, in this study, the PMMA substrate acted as an interlocking agent for the bottom layers during the heating process, firmly attaching the metal layer onto the substrate. Therefore, the presence of defects in the 3D metal nanostructures was avoided (see Figure 4). In addition, we found that the PMMA substrate became increasingly thinner when the number of layers increased. Moreover, the transmittance of the different layers was evaluated using a spectrometer (Figure 4e). The results indicated that the transparency decreased when the number of layers increased.

To demonstrate the wide applicability of the proposed method, a transparent electrode and a heater were fabricated *via* layer-by-layer nanoimprinting. Transparent electrodes are widely employed in various applications such as displays,[48,49] sensors,[50,51] and actuators.[52,53] So far, various methods have been used to fabricate these electrodes such as spray coating,[54,55] electrohydrodynamic (EHD) printing of metal grids,[54] and laser irradiation and acid dipping.[56,57] Among them, spray coating is one of the most commonly used methods for the fabrication of transparent electrodes. However, it is difficult to control the transparency, resistance, and uniformity using this method. Even though numerous researchers have attempted to control these parameters using a nanomesh structure, fabricating large-area nanomesh structures at a low cost and *via* a simple process is still challenging because the procedures involve complex and multiple fabrication steps such as electroplating, photoresist striping,[58] and molding process.[59] In this work, nanomeshes with different square sizes—400, 600, 800, and 1600 nm—were fabricated using our method, as shown in Figures 5a–d. The detailed fabrication process of the mesh nanostructures is shown in Figure S5. The related explanation is provided in the Supporting Information. The 1600 nm × 1600 nm transparent electrode produced was evaluated using a light-emitting diode (LED), as shown in Figure 5e (the flexibility of the electrode can be observed in the inset). The transmittance and sheet resistance of the fabricated samples are presented in Figures 6f and 6g, respectively. The results showed that the transparency and sheet resistance increased as the nanomesh size increased. In addition, a transparent nanoheater was fabricated and evaluated; Figure 5h presents the infrared (IR) images and properties of the fabricated nanoheater. The IR image at approximately 50 °C is displayed in Figure 5h-i. Figure 5h-ii shows that the temperature varies with the change of power density under constant time. Therefore, it is expected that the transparent nanoheater could be used on windows and side mirrors of automobiles.

To evaluate the functionality of the fabricated nanogaps, SERS was performed. As it is becoming increasingly important to detect and analyze small molecules with high sensitivity in the field of molecular diagnostics and analytical chemistry, various analytical techniques have been studied for this purpose.[60−63] Among them, SERS which uses the localized surface plasmon resonance effect of metal nanostructures is regarded as one of the most promising methods for this application because of its high specificity and sensitivity to small molecules.[64−66] For precise SERS analysis, it is important to properly position the target molecules on the SERS substrate.[67] Particularly for small molecules in dilute solutions that are difficult to detect, the signal can be amplified up to 1015 times by placing them at a sub-10 nm distance (hot spot) from the metallic nanostructure.[68] Therefore, various nanogap-based SERS substrates such as nanoparticles,[69] vertically aligned nanorod arrays,[70] nanoshells,[71] and nanopillars[72,73] have been actively studied to conveniently place the target molecules on the hot spot. However, it is still challenging to fabricate uniform and controllable nanogap structures using conventional lithography methods. Thus, the controllable, highly uniform, defect-free metal nanogap structure developed in this study can be utilized as an excellent SERS substrate.

Figure 6 shows the performance of the nanogap structures developed in this study as SERS substrates. As shown in Figure 6a, when the target molecule on the substrate is irradiated with the laser, the signal of the Raman scattered light is amplified by the strong plasmon resonance at the nanogaps. In this experiment, rhodamine 6G (R6G), a highly fluorescent material commonly used as a tracer dye for biomolecules, was used as the target molecule, and 4-aminothiophenol (4-ATP) was used as a spacer to optimize the distance between the metal and R6G.[74] In addition, the average enhancement factor (AEF) was calculated to quantitatively compare the amplification effects. This factor represents the degree of signal amplification by the nanostructures compared with that by the R6G film. It is defined as

$$\mathrm{AEF} = I_\mathrm{SERS}/N_\mathrm{SERS} \times N_\mathrm{Film}/I_\mathrm{Film} \quad (1)$$

where $I_$SERS is the intensity of the SERS signal, $N_$SERS is the areal density of the target molecules on the SERS substrate, $N_$Film is the areal density of the R6G film on the Si wafer, and $I_$Film is the intensity of the Raman signal. Details of the AEF calculation process can be found in the study by Jeong *et al.*[62] As shown in Figure 6b, the AEFs of the one-layer and two-layer Au lines are 3.9×10^2 and 2.0×10^3, respectively, which is ascribed to the amplifying effect of the Raman scattering signal by the plasmon resonance of the Au nanostructures. Notably, the AEF of the two-layer Au line was 5.24 times greater than that of the one-layer Au line because of the hot spot effect at the nanogap structure. Moreover, the AEFs of the one-layer and two-layer Ag lines were 1.4×10^4 and 3.0×10^4, respectively, as shown in Figure 6c. The AEFs of the one-layer and two-layer Ag structures were found to be 35.9 and 14.78 times greater than those of the respective Au structures, which were caused by the differences between the dielectric constants and intrinsic loss of the two metals, as reported in the literature. In contrast, the

https://dx.doi.org/10.1021/acsnano.0c05290
ACS Nano 2021, 15, 503−514

developed nanogap array allowed uniform and reliable Raman signal detection. Figure 4d shows the FIB-SEM images at five different points of the nanogap substrate; it can be seen that the average nanogap spacing of each of the five regions is highly uniform. This implies that the target molecules can uniformly cover the entire substrate and can be amplified with a relative standard deviation (RSD) within 11.3%, as shown in Figure 6e. Compared with commercially available SERS substrates that present an RSD of approximately 20% to 50%, the developed nanogap array is highly uniform and can be used as a reliable SERS substrate.[62] In summary, the developed large-area, uniform nanogap array has regular and dense hot spots and can be effectively applied to Raman spectroscopy analysis.

CONCLUSION

In summary, a simple method for fabricating wafer-scale nanogaps on flexible substrates *via* layer-by-layer nanoimprinting was proposed. The nanogaps ranging from approximately 1 to 40 nm could be controlled by adjusting the pressure, heating time, and heating temperature during the fabrication process. Ultrasmall nanogaps were observed *via* HRTEM. In addition, multilayer, 3D nanostructures with 2, 3, 5, 7, and 20 layers and without any defects were fabricated by employing layer-by-layer nanoimprinting and nanowelding technology. Moreover, a transparent electrode and a nanoheater were fabricated and evaluated *via* the proposed method. Lastly, the size-controlled, highly uniform, defect-free, ultrasmall metal nanogap structures developed were used as excellent SERS substrates; the experiment results indicated that the fabricated wafer-scale SERS substrate presented a better performance than conventional substrates. Therefore, we believe that our method can be of high significance for detecting small molecules and in manufacturing flexible electronics and soft actuators.

EXPERIMENTAL SECTION

Silicon masters with various designs were fabricated *via* KrF lithography. A resin with low surface energy (RM 311 resin) was chosen to replicate the polymer mold because a relatively low surface energy can make the metal nanopatterns easily detach and transfer onto the receiver substrate (PMMA). Polyethylene terephthalate (PET) with the polymer nanopatterns was used to fabricate the metal nanostructures that acted as the donor substrate. To replicate the nanopatterns of the Si master, first, the prepared Si master was coated with nanoimprint resin (see Figure 1a[1 and 2]), the surface of the PET film was covered with resin, and rolling was performed to improve the permeation of the imprinted resin into the nanopatterns of the Si master (see Figure 1a[2]). Second, UV-curing was performed for 90 s at two times to fully polymerize the resin (see Figure 1a[3]). Here, first, UV-curing was performed to form the polymer mold and easily separate it from the Si master. Because the separated polymer mold cannot receive UV irradiation directly, the polymer mold could not be fully polymerized. Therefore, a second direct irradiation was performed to completely polymerize the polymer mold. Then, the PET film with nanopatterns was detached from the Si master, thereby obtaining the polymer mold (see Figure 1a[4]). Note that the surface of the Si master had to be treated using a self-assembled monolayer (SAM) to allow easy detachment of the polymer mold. Trichloro(1H,1H,2H,2H-perfluorooctyl)silane was selected as the SAM treatment material (Sigma-Aldrich). Third, the metals (Ag and Au) were deposited onto the polymer mold using e-beam evaporation (DAEKI HIOTECH Co. Ltd., Korea; see Figure 1a[5]). Fourth, the fabricated Au nanowires were transferred onto the PMMA film by heating above the *Tg* of the material (110 °C) at 6 bar for 5 min. After cooling for 5 min, the PET substrate with nanopatterns was separated from the PMMA film (Figure 1a[6]), thereby obtaining Au nanowires fabricated on the PMMA film. Fifth, a second layer of Au nanowires was transferred onto the PMMA film by heating above the *Tg* of the material (110 °C) at 1 bar for 2 min to form the cross nanostructures with nanogaps (Figure 1a[7]). The process was implemented using thermal nanoimprinting equipment, the schematic of which is provided in Figure S6. The samples with one and two layers were evaluated by field emission scanning electron microscopy (FE-SEM; Sirion, FEI, Netherlands) and FIB technology (Helios Nanolab, FEI, Netherlands), respectively. To further confirm the sizes of the nanogaps, TEM (JEM-ARM200F, JEOL, Japan) was performed. A spectrometer (QE Pro 6000, Ocean Optics, USA) was used to measure the dependence of transmittance on the number of layers of the fabricated nanostructures. In addition, SERS results of the fabricated nanostructures were evaluated.

For SERS, the nanogap structures were coated with 4-aminothiophenol (422967, Sigma-Aldrich, USA) and rhodamine 6G (56226, Sigma-Aldrich, USA). First, the fabricated nanogap substrates were immersed in a 1×10^{-6} M 4-ATP ethanolic solution and then rinsed with ethanol to remove the excess coating molecules. Second, a 1×10^{-6} M rhodamine 6G solution was poured onto the substrate with a surface of 1 cm^2 to form a 27-μm-thick layer, and the solvent was dried afterward. Finally, the SERS signal was measured using a dispersive Raman spectrometer (ARAMIS, Horiba Jobin Yvon, France) with a 644-nm laser. The Raman signal was recorded for 15 and 2 s for Au and Ag, respectively. For AEF and RSD evaluation, the representative rhodamine 6G peaks at 635, 1075, 1170, 1577, and 1649 nm were used, and the PMMA substrate peaks were removed during SERS detection for baseline correction.

ASSOCIATED CONTENT

Supporting Information

The Supporting Information is available free of charge at https://pubs.acs.org/doi/10.1021/acsnano.0c05290.

Large-area photo of nanogap substrate with standard ruler (Figure S1); detailed conditions of experiments performed in research (Table S1); TEM cross-sectional images of fabricated nanogaps depending on heating temperature, heating time, and pressures (Figure S2); focused ion beam and HRTEM morphologies and cross-sectional images of nanogaps of different thicknesses (Figure S3); HRTEM cross-sectional images of nanostructures with three layers (Figure S4); fabrication process of nanomesh structure (Figure S5); and thermal nanoimprinting equipment (Figure S6) (PDF)

AUTHOR INFORMATION

Corresponding Authors

Jun-Ho Jeong − *Nano-Convergence Mechanical Systems Research Division, Korea Institute of Machinery and Materials, Daejeon 34103, South Korea; Department of Nano Mechatronics, University of Science and Technology, Daejeon 34103, South Korea;* orcid.org/0000-0003-0671-0225; Email: jhjeong@kimm.re.kr

Inkyu Park − *Department of Mechanical Engineering, Korea Advanced Institute of Science and Technology, Daejeon 34141, South Korea;* orcid.org/0000-0001-5761-7739; Email: inkyu@kaist.ac.kr

Authors

Zhi-Jun Zhao − *Nano-Convergence Mechanical Systems Research Division, Korea Institute of Machinery and Materials, Daejeon 34103, South Korea*

Junseong Ahn − *Nano-Convergence Mechanical Systems Research Division, Korea Institute of Machinery and*

https://dx.doi.org/10.1021/acsnano.0c05290
ACS Nano 2021, 15, 503−514

Materials, Daejeon 34103, South Korea; Department of Mechanical Engineering, Korea Advanced Institute of Science and Technology, Daejeon 34141, South Korea

Soon Hyoung Hwang − *Nano-Convergence Mechanical Systems Research Division, Korea Institute of Machinery and Materials, Daejeon 34103, South Korea*

Jiwoo Ko − *Nano-Convergence Mechanical Systems Research Division, Korea Institute of Machinery and Materials, Daejeon 34103, South Korea; Department of Mechanical Engineering, Korea Advanced Institute of Science and Technology, Daejeon 34141, South Korea*

Yongrok Jeong − *Nano-Convergence Mechanical Systems Research Division, Korea Institute of Machinery and Materials, Daejeon 34103, South Korea*

Moonjeong Bok − *Nano-Convergence Mechanical Systems Research Division, Korea Institute of Machinery and Materials, Daejeon 34103, South Korea*

Hyeok-Joong Kang − *Nano-Convergence Mechanical Systems Research Division, Korea Institute of Machinery and Materials, Daejeon 34103, South Korea*

Jungrak Choi − *Department of Mechanical Engineering, Korea Advanced Institute of Science and Technology, Daejeon 34141, South Korea*

Sohee Jeon − *Nano-Convergence Mechanical Systems Research Division, Korea Institute of Machinery and Materials, Daejeon 34103, South Korea*

Complete contact information is available at: https://pubs.acs.org/10.1021/acsnano.0c05290

Author Contributions

Z.-J.Z. and J.A. contributed equally. The manuscript was written through contributions of all authors. All authors have given approval to the final version of the manuscript.

Notes

The authors declare no competing financial interest.

ACKNOWLEDGMENTS

This work was supported by the Center for Advanced Metamaterials (CAMM) funded by the Ministry of Science, ICT and Future Planning, Korea, through the Global Frontier Project (CAMM-No. 2014M3A6B3063707), Institute of Information & Communications Technology Planning & Evaluation (IITP) grant funded by the Korea government (MSIT) (No. 2020-0-00831, Development of holographic lithography equipment and printing technology for security and books) and the Basic Research Program of KIMM (Korea Institute of Machinery and Materials, NK224C), and a National Research Foundation of Korea (NRF) grant funded by the Korean government (MSIT) [No. 2018R1A2B2004910].

REFERENCES

(1) Lei, D. Y.; Appavoo, K.; Ligmajer, F.; Sonnefraud, Y.; Haglund, R. F., Jr.; Maier, S. A. Optically-Triggered Nanoscale Memory Effect in a Hybrid Plasmonic-Phase Changing Nanostructure. *ACS Photonics* **2015**, *2*, 1306−1313.

(2) Ross, M. B.; Mirkin, C. A.; Schatz, G. C. Optical Properties of One-, Two-, and Three-Dimensional Arrays of Plasmonic Nanostructures. *J. Phys. Chem. C* **2016**, *120*, 816−830.

(3) Rahman, M. M.; Jamal, A.; Khan, S. B.; Faisal, M. CuO Codoped ZnO Based Nanostructured Materials for Sensitive Chemical Sensor Applications. *ACS Appl. Mater. Interfaces* **2011**, *3*, 1346−1351.

(4) Valsecchi, C.; Brolo, A. G. Periodic Metallic Nanostructures as Plasmonic Chemical Sensors. *Langmuir* **2013**, *29*, 5638−5649.

(5) Luk'yanchuk, B.; Zheludev, N. I.; Maier, S. A.; Halas, N. J.; Nordlander, P.; Giessen, H.; Chong, C. T. The Fano Resonance in Plasmonic Nanostructures and Metamaterials. *Nat. Mater.* **2010**, *9*, 707−715.

(6) Kneipp, K.; Wang, Y.; Kneipp, H.; Perelman, L. T.; Itzkan, I.; Dasari, R. R.; Feld, M. S. Single Molecule Detection Using Surface-Enhanced Raman Scattering (SERS). *Phys. Rev. Lett.* **1997**, *78*, 1667.

(7) Sawai, Y.; Takimoto, B.; Nabika, H.; Ajito, K.; Murakoshi, K. Observation of a Small Number of Molecules at a Metal Nanogap Arrayed on a Solid Surface Using Surface-Enhanced Raman Scattering. *J. Am. Chem. Soc.* **2007**, *129*, 1658−1662.

(8) Talley, C. E.; Jackson, J. B.; Oubre, C.; Grady, N. K.; Hollars, C. W.; Lane, S. M.; Huser, T. R.; Nordlander, P.; Halas, N. J. Surface-Enhanced Raman Scattering from Individual Au Nanoparticles and Nanoparticle Dimer Substrates. *Nano Lett.* **2005**, *5*, 1569−1574.

(9) Glass, R.; Arnold, M.; Blümmel, J.; Küller, A.; Möller, M.; Spatz, J. P. Micro-Nanostructured Interfaces Fabricated by the Use of Inorganic Block Copolymer Micellar Monolayers as Negative Resist for Electron-Beam Lithography. *Adv. Funct. Mater.* **2003**, *13*, 569−575.

(10) Fischer, J.; von Freymann, G.; Wegener, M. The Materials Challenge in Diffraction-Unlimited Direct-Laser-Writing Optical Lithography. *Adv. Mater.* **2010**, *22*, 3578−3582.

(11) Zhang, Y. L.; Chen, Q. D.; Xia, H.; Sun, H. B. Designable 3D Nanofabrication by Femtosecond Laser Direct Writing. *Nano Today* **2010**, *5*, 435−448.

(12) Menard, E.; Bilhaut, L.; Zaumseil, J.; Rogers, J. A. Improved Surface Chemistries, Thin Film Deposition Techniques, and Stamp Designs for Nanotransfer Printing. *Langmuir* **2004**, *20*, 6871−6878.

(13) Zheng, C.; Shen, Y.; Liu, M.; Liu, W.; Wu, S.; Jin, C. Layer-by-Layer Assembly of Three-Dimensional Optical Functional Nanostructures. *ACS Nano* **2019**, *13*, 5583−5590.

(14) Hwang, S. H.; Jeon, S.; Kim, M. J.; Choi, D. G.; Choi, J. K.; Jung, J. Y.; Kim, K. S.; Lee, J.; Jeong, J. H.; Youn, J. R. Covalent Bonding-Assisted Nanotransfer Lithography for the Fabrication of Plasmonic Nano-Optical Elements. *Nanoscale* **2017**, *9*, 14335−14346.

(15) Jeong, J. W.; Yang, S. R.; Hur, Y. R.; Kim, S. W.; Baek, K. M.; Yim, S.; Jang, H. I.; Park, J. H.; Lee, S. Y.; Park, C. O.; Jung, Y. S. High-Resolution Nanotransfer Printing Applicable to Diverse Surfaces *via* Interface-Targeted Adhesion Switching. *Nat. Commun.* **2014**, *5*, 5387.

(16) Seo, M. H.; Choi, S. J.; Park, S. H.; Yoo, J. Y.; Lim, S. K.; Lee, J. S.; Choi, K. W.; Jo, M. S.; Kim, I. D.; Yoon, J. B. Material-Independent Nanotransfer onto a Flexible Substrate Using Mechanical-Interlocking Structure. *ACS Nano* **2018**, *12*, 4387−4397.

(17) Liu, K.; Bai, Y.; Zhang, L.; Yang, Z.; Fan, Q.; Zheng, H.; Yin, Y.; Gao, C. Porous Au−Ag Nanospheres with High-Density and Highly Accessible Hotspots for SERS Analysis. *Nano Lett.* **2016**, *16*, 3675−3681.

(18) Das, G.; Mecarini, F.; Gentile, F.; De Angelis, F.; Kumar, M. H. G.; Candeloro, P.; Liberale, C.; Cuda, G.; Di Fabrizio, E. Nano-Patterned SERS Substrate: Application for Protein Analysis *vs.* Temperature. *Biosens. Bioelectron.* **2009**, *24*, 1693−1699.

(19) Alvarez-Puebla, R. A.; Liz-Marzán, L. M. SERS-Based Diagnosis and Biodetection. *Small* **2010**, *6*, 604−610.

(20) Kuttner, C.; Mayer, M.; Dulle, M.; Moscoso, A.; López-Romero, J. M.; Förster, S.; Fery, A.; Pérez-Juste, J.; Contreras-Cáceres, R. Seeded Growth Synthesis of Gold Nanotriangles: Size Control, SAXS Analysis, and SERS Performance. *ACS Appl. Mater. Interfaces* **2018**, *10*, 11152−11163.

(21) Atanasov, P. A.; Nedyalkov, N. N.; Fukata, N.; Jevasuwan, W.; Subramani, T.; Hirsch, D.; Rauschenbach, B. Au and Ag Films and Nanostructures for Detection of Fungicide Mancozeb: SERS Analyses. *AIP Conf. Proc.* **2018**, *2075*, No. 030001.

(22) Heck, C.; Kanehira, Y.; Kneipp, J.; Bald, I. Amorphous Carbon Generation As a Photocatalytic Reaction on DNA-Assembled Gold and Silver Nanostructures. *Molecules* **2019**, *24*, 2324.

(23) Murphy, C. J.; Gole, A. M.; Hunyadi, S. E.; Orendorff, C. J. One-Dimensional Colloidal Gold and Silver Nanostructures. *Inorg. Chem.* **2006**, *45*, 7544−7554.
(24) Tian, Z. Q.; Ren, B.; Wu, D. Y. Surface-Enhanced Raman Scattering: From Noble to Transition Metals and From Rough Surfaces to Ordered Nanostructures. *J. Phys. Chem. B* **2002**, *106*, 9463−9483.
(25) Im, H.; Bantz, K. C.; Lee, S. H.; Johnson, T. W.; Haynes, C. L.; Oh, S. H. Self-Assembled Plasmonic Nanoring Cavity Arrays for SERS and LSPR Biosensing. *Adv. Mater.* **2013**, *25*, 2678−2685.
(26) Zuo, Z.; Zhang, S.; Wang, Y.; Guo, Y.; Sun, L.; Li, K.; Cui, G. Effective Plasmon Coupling in Conical Cavities for Sensitive Surface Enhanced Raman Scattering with Quantitative Analysis Ability. *Nanoscale* **2019**, *11*, 17913−17919.
(27) Gisbert Quilis, N.; Lequeux, M.; Venugopalan, P.; Khan, I.; Knoll, W.; Boujday, S.; de la Chapellebe, M. L.; Dostalek, J. Tunable Laser Interference Lithography Preparation of Plasmonic Nanoparticle Arrays Tailored for SERS. *Nanoscale* **2018**, *10*, 10268−10276.
(28) Li, J.; Deng, T. S.; Liu, X.; Dolan, J. A.; Scherer, N. F.; Nealey, P. F. Hierarchical Assembly of Plasmonic Nanoparticle Heterodimer Arrays with Tunable Sub-5 nm Nanogaps. *Nano Lett.* **2019**, *19*, 4314−4320.
(29) Nam, N. N.; Bui, T. L.; Son, S. J.; Joo, S. W. Ultrasonication-Induced Self-Assembled Fixed Nanogap Arrays of Monomeric Plasmonic Nanoparticles inside Nanopores. *Adv. Funct. Mater.* **2019**, *29*, 1809146.
(30) Im, H.; Bantz, K. C.; Lindquist, N. C.; Haynes, C. L.; Oh, S. H. Vertically Oriented Sub-10-nm Plasmonic Nanogap Arrays. *Nano Lett.* **2010**, *10*, 2231−2236.
(31) Ma, C.; Gao, Q.; Hong, W.; Fan, J.; Fang, J. Real-Time Probing Nanopore-in-Nanogap Plasmonic Coupling Effect on Silver Supercrystals with Surface-Enhanced Raman Spectroscopy. *Adv. Funct. Mater.* **2017**, *27*, 1603233.
(32) Kim, H. Y.; Kim, K. S.; Kim, B. H. Micro/Nano Patterning Characteristics in Hot Embossing Process. *AIP Conf. Proc.* **2004**, *712*, 1470.
(33) Zhou, W.; Min, G.; Zhang, J.; Liu, Y.; Wang, J.; Zhang, Y.; Sun, F. Nanoimprint Lithography: A Processing Technique for Nanofabrication Advancement. *Nano-Micro Lett.* **2011**, *3*, 135−140.
(34) Cho, W. K.; Yeo, N. E.; Kang, J. S.; Kim, D. I.; Jeong, M. Y. Effects of Sacrificial Layer Thickness on Fidelity of Multi-Scale Hierarchical Structure Fabricated by Thermal Nanoimprint Lithography. *Nanosci. Nanotechnol. Lett.* **2018**, *10*, 1305−1309.
(35) Ferriol, M.; Gentilhomme, A.; Cochez, N.; Oget, N.; Mieloszynski, J. L. Thermal Degradation of Poly (Methyl Methacrylate) (PMMA): Modelling of DTG and TG Curves. *Polym. Degrad. Stab.* **2003**, *79*, 271−281.
(36) Roth, C. B.; Dutcher, J. R. Glass Transition Temperature of Freely-Standing Films of Atactic Poly (Methyl Methacrylate). *Eur. Phys. J. E: Soft Matter Biol. Phys.* **2003**, *12*, 103−107.
(37) Zhao, Z. J.; Hwang, S. H.; Kang, H. J.; Jeon, S.; Bok, M.; Ahn, S.; Im, D.; Hahn, J.; Kim, H.; Jeong, J. H. Adhesive-Layer-Free and Double-Faced Nanotransfer Lithography for Flexible Large-Area Meta-Surface Hologram. *ACS Appl. Mater. Interfaces* **2020**, *12*, 1737.
(38) Zhu, S.; Li, H.; Yang, M.; Pang, S. W. High Sensitivity Plasmonic Biosensor Based on Nanoimprinted Quasi 3D Nanosquares for Cell Detection. *Nanotechnology* **2016**, *27*, 295101.
(39) Guo, L.; Chen, G.; Kim, D. W. Three-Dimensionally Assembled Gold Nanostructures for Plasmonic Biosensors. *Anal. Chem.* **2010**, *82*, 5147−5153.
(40) Qiao, Y.; Li, C. M. Nanostructured Catalysts in Fuel Cells. *J. Mater. Chem.* **2011**, *21*, 4027−4036.
(41) Zečević, J.; de Jong, K. P.; de Jongh, P. E. Progress in Electron Tomography to Assess the 3D Nanostructure of Catalysts. *Curr. Opin. Solid State Mater. Sci.* **2013**, *17*, 115−125.
(42) Liaw, J. W.; Chien, C. W.; Liu, K. C.; Ku, Y. C.; Kuo, M. K. 3D Optical Vortex Trapping of Plasmonic Nanostructure. *Sci. Rep.* **2018**, *8*, 12673.
(43) Loo, Y. L.; Lang, D. V.; Rogers, J. A.; Hsu, J. W. Electrical Contacts to Molecular Layers by Nanotransfer Printing. *Nano Lett.* **2003**, *3*, 913−917.
(44) Zaumseil, J.; Meitl, M. A.; Hsu, J. W.; Acharya, B. R.; Baldwin, K. W.; Loo, Y. L.; Rogers, J. A. Three-Dimensional and Multilayer Nanostructures Formed by Nanotransfer Printing. *Nano Lett.* **2003**, *3*, 1223−1227.
(45) Chanda, D.; Shigeta, K.; Gupta, S.; Cain, T.; Carlson, A.; Mihi, A.; Baca, J. A.; Bogart, G. R.; Braun, P.; Rogers, J. A. Large-Area Flexible 3D Optical Negative Index Metamaterial Formed by Nanotransfer Printing. *Nat. Nanotechnol.* **2011**, *6*, 402−407.
(46) Zhao, Z. J.; Shin, S. H.; Choi, D. G.; Park, S. H.; Jeong, J. H. Shape-Controlled 3D Periodic Metal Nanostructures Fabricated *via* Nanowelding. *Small* **2018**, *14*, 1703102.
(47) Zhao, Z. J.; Gao, M.; Hwang, S.; Jeon, S.; Park, I.; Park, S. H.; Jeong, J. H. Heterogeneous Nanostructures Fabricated *via* Binding Energy-Controlled Nanowelding. *ACS Appl. Mater. Interfaces* **2019**, *11*, 7261−7271.
(48) Pellerite, M. J.; Radcliffe, M. D.; Baetzold, J. P.; Boulos, M. A.; Steiner, M. L.; Stradinger, J. J. *Transparent Electrode for Electronic Displays*; U.S. Patent No. 10101617B2, 2018.
(49) Zhang, H.; Teramoto, S. *Display Device Including a Transparent Electrode Pattern Covering and Extending along Gate & Source Lines*; U.S. Patent No. 6421101B1, 2002.
(50) Song, J. K.; Son, D.; Kim, J.; Yoo, Y. J.; Lee, G. J.; Wang, L.; Choi, M. K.; Yang, J.; Lee, M.; Do, K.; Koo, J. H.; Lu, N.; Kim, J. H.; Hyeon, T.; Song, Y. M.; Kim, D. H. Wearable Force Touch Sensor Array Using a Flexible and Transparent Electrode. *Adv. Funct. Mater.* **2017**, *27*, 1605286.
(51) Okazaki, T.; Shiokawa, E.; Orii, T.; Yamamoto, T.; Hata, N.; Taguchi, A.; Sugawara, K.; Kuramitz, H. Simultaneous Multiselective Spectroelectrochemical Fiber-Optic Sensor: Sensing with an Optically Transparent Electrode. *Anal. Chem.* **2018**, *90*, 2440−2445.
(52) Shian, S.; Diebold, R. M.; Clarke, D. R. Tunable Lenses Using Transparent Dielectric Elastomer Actuators. *Opt. Express* **2013**, *21*, 8669−8676.
(53) Jun, K.; Kim, J.; Oh, I. K. An Electroactive and Transparent Haptic Interface Utilizing Soft Elastomer Actuators with Silver Nanowire Electrodes. *Small* **2018**, *14*, 1801603.
(54) Selzer, F.; Weiß, N.; Kneppe, D.; Bormann, L.; Sachse, C.; Gaponik, N.; Eychmüller, A.; Leo, K.; Müller-Meskamp, L. A Spray-Coating Process for Highly Conductive Silver Nanowire Networks as the Transparent Top-Electrode for Small Molecule Organic Photovoltaics. *Nanoscale* **2015**, *7*, 2777−2783.
(55) Kim, T.; Canlier, A.; Kim, G. H.; Choi, J.; Park, M.; Han, S. M. Electrostatic Spray Deposition of Highly Transparent Silver Nanowire Electrode on Flexible Substrate. *ACS Appl. Mater. Interfaces* **2013**, *5*, 788−794.
(56) Lee, Y.; Jin, W. Y.; Cho, K. Y.; Kang, J. W.; Kim, J. Thermal Pressing of a Metal-Grid Transparent Electrode into a Plastic Substrate for Flexible Electronic Devices. *J. Mater. Chem. C* **2016**, *4*, 7577−7583.
(57) Tran, N. H.; Duong, T. H.; Kim, H. C. A Fast Fabrication of Copper Nanowire Transparent Conductive Electrodes by Using Pulsed Laser Irradiation. *Sci. Rep.* **2017**, *7*, 15093.
(58) Khan, A.; Lee, S.; Jang, T.; Xiong, Z.; Zhang, C.; Tang, J.; Guo, L. J.; Li, W. D. High-Performance Flexible Transparent Electrode with an Embedded Metal Mesh Fabricated by Cost-Effective Solution Process. *Small* **2016**, *12*, 3021−3030.
(59) Kang, M. G.; Park, H. J.; Ahn, S. H.; Guo, L. J. Transparent Cu Nanowire Mesh Electrode on Flexible Substrates Fabricated by Transfer Printing and Its Application in Organic Solar Cells. *Sol. Energy Mater. Sol. Cells* **2010**, *94*, 1179−1184.
(60) Kelley, S. O.; Mirkin, C. A.; Walt, D. R.; Ismagilov, R. F.; Toner, M.; Sargent, E. H. Advancing the Speed, Sensitivity and Accuracy of Biomolecular Detection Using Multi-Length-Scale Engineering. *Nat. Nanotechnol.* **2014**, *9*, 969−980.
(61) Kosaka, P. M.; Pini, V.; Ruz, J. J.; da Silva, R. A.; González, M. U.; Ramos, D.; Calleja, M.; Tamayo, J. Detection of Cancer

Biomarkers in Serum Using a Hybrid Mechanical and Optoplasmonic Nanosensor. *Nat. Nanotechnol.* **2014**, *9*, 1047−1053.
(62) Zhou, L.; Ding, F.; Chen, H.; Ding, W.; Zhang, W.; Chou, S. Y. Enhancement of lmmunoassay's Fluorescence and Detection Sensitivity Using Three-Dimensional Plasmonic Nano-Antenna-Dots Array. *Anal. Chem.* **2012**, *84*, 4489−4495.
(63) Zhang, W.; Ding, F.; Li, W. D.; Wang, Y.; Hu, J.; Chou, S. Y. Giant and Uniform Fluorescence Enhancement over Large Areas Using Plasmonic Nanodots in 3D Resonant Cavity Nanoantenna by Nanoimprinting. *Nanotechnology* **2012**, *23*, 225301.
(64) Li, J. F.; Huang, Y. F.; Ding, Y.; Yang, Z. L.; Li, S. B.; Zhou, X. S.; Fan, F. R.; Zhang, W.; Zhou, Z. Y.; Wu, D. Y.; Ren, B.; Wang, Z. L.; Tian, Z. Q. Shell-Isolated Nanoparticle-Enhanced Raman Spectroscopy. *Nature* **2010**, *464*, 392−395.
(65) De Angelis, F.; Gentile, F.; Mecarini, F.; Das, G.; Moretti, M.; Candeloro, P.; Coluccio, M. L.; Cojoc, G.; Accardo, A.; Liberale, C.; Zaccaria, R. P.; Perozziello, G.; Tirinato, L.; Toma, A.; Cuda, G.; Cingolani, R.; Di Fabrizio, E. Breaking the Diffusion Limit with Super-Hydrophobic Delivery of Molecules to Plasmonic Nanofocusing SERS Structures. *Nat. Photonics* **2011**, *5*, 682−687.
(66) Cecchini, M. P.; Turek, P. A.; Paget, J.; Kornyshev, A. A.; Edel, J. B. Self-Assembled Nanoparticle Arrays for Multiphase Trace Analyte Detection. *Nat. Mater.* **2013**, *12*, 165−171.
(67) Willets, K. A.; Van Duyne, R. P. Localized Surface Plasmon Resonance Spectroscopy and Sensing. *Annu. Rev. Phys. Chem.* **2007**, *58*, 267−297.
(68) Jeong, J. W.; Arnob, M. M. P.; Baek, K. M.; Lee, S. Y.; Shih, W. C.; Jung, Y. S. 3D Cross-Point Plasmonic Nanoarchitectures Containing Dense and Regular Hot Spots for Surface-Enhanced Raman Spectroscopy Analysis. *Adv. Mater.* **2016**, *28*, 8695−8704.
(69) Lim, D. K.; Jeon, K. S.; Hwang, J. H.; Kim, H.; Kwon, S.; Suh, Y. D.; Nam, J. M. Highly Uniform and Reproducible Surface-Enhanced Raman Scattering From DNA-Tailorable Nanoparticles with 1-nm Interior Gap. *Nat. Nanotechnol.* **2011**, *6*, 452−460.
(70) Thai, T.; Zheng, Y.; Ng, S. H.; Mudie, S.; Altissimo, M.; Bach, U. Self-Assembly of Vertically Aligned Gold Nanorod Arrays on Patterned Substrates. *Angew. Chem., Int. Ed.* **2012**, *51*, 8732−8735.
(71) Yang, S.; Cai, W.; Kong, L.; Lei, Y. Surface Nanometer-Scale Patterning in Realizing Large-Scale Ordered Arrays of Metallic Nanoshells with Well-Defined Structures and Controllable Properties. *Adv. Funct. Mater.* **2010**, *20*, 2527−2533.
(72) Li, W. D.; Ding, F.; Hu, J.; Chou, S. Y. Three-Dimensional Cavity Nanoantenna Coupled Plasmonic Nanodots for Ultrahigh and Uniform Surface-Enhanced Raman Scattering over Large Area. *Opt. Express* **2011**, *19*, 3925−3936.
(73) Zang, F.; Su, Z.; Zhou, L.; Konduru, K.; Kaplan, G.; Chou, S. Y. Ultrasensitive Ebola Virus Antigen Sensing *via* 3D nanoantenna arrays. *Adv. Mater.* **2019**, *31*, 1902331.
(74) Liu, G.; Zheng, H.; Liu, M.; Zhang, Z.; Dong, J.; Yan, X.; Li, X. Surface-Enhanced Fluorescence of Rhodamine 6G on the Assembled Silver Nanostructures. *J. Nanosci. Nanotechnol.* **2011**, *11*, 9523−9527.

https://dx.doi.org/10.1021/acsnano.0c05290
ACS Nano 2021, 15, 503−514